Microstructure and mechanical properties of Cu\Ni-coated α-Al_2O_{3w} and graphene nano-platelets co-reinforced copper matrix composites

Zhijian Li [a,b], Xiaosong Jiang[a,b], Hongliang Sun[a,b],Sipeng Liu[b], Yong Pang[c*] , Zixuan Wu[d], Liu Yang[e]*

[a]Key Laboratory of Advanced Technologies of Materials, Ministry of Education, Chengdu 610031, China

[b]School of Materials Science and Engineering, Southwest Jiaotong University, Chengdu Sichuan 610031, China

[c]School of Materials Science and Engineering, Central South University, Changsha, 410083, China

[d]School of Engineering and Materials Science, Queen Mary University of London, London E1 4NS, United Kingdom

[e]Institute for Applied Materials (IAM-WK), Karlsruhe Institute of Technology (KIT), Karlsruhe 76131, Germany

*Corresponding author: xsjiang@swjtu.edu.cn (X.S. Jiang) OR thgink@126.com (Y. Pang).

Abstract: graphene nano-platelets (GNPs) and α-Al_2O_{3w} reinforced laminated Cu matrix composites were successfully prepared by flake powders metallurgy (FPM) and vacuum hot pressing sintering. In order to compare the effects of different coatings on the interfacial and mechanical properties, Cu\Ni-coated were used for surface modification of reinforcement surface. The microstructure, interfacial bonding and mechanical properties of Cu\Ni-coated GNPs and α-Al_2O_{3w} co-enhanced laminated Cu matrix composites were investigated. The results showed that composites with Cu coating on the surface of reinforcement had poor contact and lower mechanical properties. In contrast, the introduction of Ni coating improved interfacial bonding and also brought

about solid solution strengthening of matrix. When the content of Ni coating GNPs was 1 wt.%, tensile strength reached 336.12 MPa and elongation was 16.36%. On the one hand, the Ni coating promoted interfacial bonding, and good interface brings better load transfer and interfacial strength. Meanwhile, α-Al_2O_{3w} and GNPs with different aspect ratios showed better strengthening effects through various strengthening modes such as drawing and fracture. On the other hand, the laminated structure allowed crack extension to be transferred to other planes, the crack deflection process consumes more energy, and composite achieves a balance of strength and toughness. This work provides a new idea to improve interfacial bonding of composites and obtain high strength and toughness.

Keywords: Laminated composites; Cu\Ni-coated; Graphene nano-platelets; α-Al_2O_{3w}; Mechanical properties

Introduction

Copper matrix composites are widely used as engineering materials due to their high tensile strength, high Young's modulus, good electrical, thermal conductivity, and excellent wear resistance [1-3]. In recent years, with the development of material science, more and more new materials have been discovered and used as reinforcement to strengthen metal matrix composites [4,5]. Graphene nanoplatelets (GNPs), as a two-dimensional material with a special structure, are considered to be one of the most promising reinforcement due to their high strength and excellent physical properties [6-8]. In order to obtain composites with good overall performance, multiphase reinforced hybrid reinforced composites have become a hot research topic in recent years [9]. As an important ceramic reinforcement, α-Al_2O_{3w} has gained wide attention due to its special fibrous structure, high strength and high chemical stability [5,10]. The fibrillated whiskers are a key component of the material. The failure mode of fibrous whiskers during material fracture is divided into two modes: pull-out and fracture.[11,12]. Meanwhile, it was recently shown that the GNPs would hinder the crack expansion path when α-Al_2O_{3w}/Cu interfacial microcracks expand along the interface [13]. The GNPs in composites are used to enhance the reinforcement effect of α-Al_2O_{3w}, thus playing a '1+1>2' role. Although composites can improve the performance of matrix, poor interfacial compatibility and different coefficients of thermal expansion also limit the development of composites to some extent [14,15].

To improve the interfacial bonding, many studies have focused on improving the interfacial compatibility through surface modification methods. Such as salt bath method [16] physical vapor deposition (PVD) method [17] and chemical vapor deposition (CVD) methods [18]. However, these methods have many drawbacks. For example, the surface modification by PVD and CVD is inefficiency, and surface-modified coating have reduced coverage and tend to expose the matrix. Electroless plating is a more efficient surface modification method with high controllability and good coverage [19]. In the current study, to improve the interfacial bonding, surface modification of reinforcement with metal elements such as Cu [20,21] , W [22] , Ni [23,24] and Ag [25] as coating has been widely investigated. Wang et al. [19] compared the flexural properties of Cu matrix composites with and without Cu coating on the surface of GNPs., they found that bending strength

of composites with Cu coating GNPs films was 56% higher than that of the uncoated composites, and the location of crack occurrence was shifted from interface to matrix. After the introduction of metallic elements into reinforcement, the wettability of interface can be greatly improved, and it was also found that coating elements can diffuse into matrix during the sintering process to form solid solution [26,27]. Li et al. [27] found that Ni coating diffused into Cu during the sintering process to form solid solution and formed solid solution reinforcement at the interface by observing elemental content on the extracted carbon nanotubes. The coating- matrix interface effectively inhibits the movement of dislocations and effectively enhances mechanical properties of material. The improved binding and wettability at the interface brings better interfacial bonding, and also improves the dispersion of reinforcement and reduces agglomeration phenomenon [28]. However, although the introduction of coating improves interfacial bonding properties and avoids premature failure of material due to defects, its enhancement of composites properties is limited and contributes less to solving contradictory problem of composite strength and toughness. In order to obtain composites with high strength and high toughness, recent studies have developed biomimetic materials with reference to biological materials with high strength and high toughness, which provide new ideas to solve problem of conflicting material strength and toughness.

The laminated structure of the pearl shell is usually composed of calcium carbonate and organic protein, where the harder calcium carbonate resembles "bricks" and the softer organic protein resembles "mud", which combine to form a "brick-mud" structure [29,30]. This structure brings multiple strengthening mechanisms and multi-scale toughening mechanisms to achieve a good strength and toughness fit. Inspired by such biomaterials, a lot of research in recent years has focused on the preparation of composites with uniformly dispersed reinforcement and distinct laminated structures. Commonly used methods include flake powders metallurgy [20,31] freeze casting [32] and cumulative stack rolling method etc. [33] Among them, flake powders metallurgy (FPM) is method with high degree of freedom and high efficiency for preparation of laminated structure. Luo et al. [34] used method of FPM to determine optimal ball milling parameters by adjusting the ball milling parameters and comparing the specific surface area of Cu flakes under different parameters. The larger surface area of laminated metal powders than the spherical powders gives it better geometric compatibility with reinforcement and also greatly improves the adsorption capacity of reinforcement [35] . The laminated structure increases the dispersion of reinforcement and bonding

force with matrix. At the same time, laminated structure can achieve a good balance of strength and toughness. Su et al. [36] studies have shown that the contribution of laminated structure to strength is mainly due to the change of the reinforcement dispersion and alignment direction inside composites. The reinforcement distributed unidirectionally along stress in laminated composites is more favorable to load transfer than random orientation. The laminated structure facilitates the deflection and passivation of cracks and also inhibits strain localization during plastic deformation [37]. Huo's [38] study shows that during fracture of material, crack extension occurs with multiple deflections and cracks or slight delamination near brittle phase of greater thickness. Fine particles in matrix also deflect crack extension thus prolonging cracking path. Better load transfer and crack deflection and passivation result in a good match of strength and toughness of laminated composites.

As mentioned above, several methods have been investigated to enhance the comprehensive mechanical properties of Cu matrix composites, such as by improving the interfacial bond strength and changing the structure. However, less studies have been conducted to enhance the mechanical properties of Cu matrix composites by combining the method of laminated structure and chemical plating modification. In this study, to improve the interfacial bond strength, surface modification was carried out using chemical plating. Subsequently, laminated structure was built using FPM to obtain a balance of strength and toughness. Multiple methods were combined in order to better improve the mechanical properties of composites. Finally, Cu\Ni-coated α-Al_2O_{3w} and GNPs co-reinforced copper matrix composites were prepared by vacuum hot pressing sintering. The effects of different coating on the microstructure and mechanical properties of composites and interfacial bonding mechanism were analyzed, while the GNPs content with the best performance under the conditions of nickel coating was explored, composites strength and toughness coordination were optimized by the construction of the laminated structure. The results of this paper provide a theoretical basis for selecting a better coating and the optimal GNPs content to obtain Cu-GNPs-α-Al_2O_{3w} laminated composites with excellent comprehensive properties.

2. Experiment

2.1 Materials

In this study, pure Cu powders (purity 99.9%, 300 mesh) was used as matrix material. GNPs (150-180 μm), α-Al_2O_{3w} (D: 0.1-4 μm; L: 5-30 μm) were used as reinforcement. To obtain flaky Cu powders, ball milling was performed using stainless steel planetary balls with a ball-to-powders ratio of 10:1. Tert-butanol was used as the ball milling medium and ball milled at 300 rpm for 6 h. Before the experiments, the surface modification of GNPs and α-Al_2O_{3w} was electroless plating. First, the surface of reinforcement was roughened by ultrasonic shock and surface formed structure favorable for ion adsorption. Subsequently, sensitization and activation were carried out in stannous chloride and palladium chloride solutions, substance acting as an active catalyst was Pd^{2+} reduced by the sensitizing solution $SnCl_2$ to Pd^0 followed by palladium particles surrounded by a tin chloride shell layer. The sensitization solution was a mixture of $SnCl_2$ 30 g/L and HCl 60 mL/L, and the activation solution was a mixture of $PdCl_2$ 0.25 g/L and HCl 10 mL/L. Finally, coating was introduced on the surface of reinforcement by electroless plating at 35°C ambient. The main salt groups used for different electroless plating are shown in Table 1. The treated powders were mixed by ball milling for 1 h. The ball milling powders slurry was dried using a vacuum freeze dryer (FD-a-50) for 24 h to obtain desired composite powders. Composite powders were encapsulated in a circular graphite mold with a diameter of 55 mm. The graphite molds were placed in a vacuum hot press furnace (HAS-25) and heated to 650 °C at a pressure of 30 MPa at a rate of 10 °C/min, followed by holding for 90 min, and finally composites blocks were obtained by cooling with the furnace. The samples obtained in this experiment were (Cu coating) Cu-0.5 wt.% GNPs-0.5 wt.% α-Al_2O_{3w}, (Ni coating) Cu-0.5 wt.% GNPs-0.5 wt.% α-Al_2O_{3w}, (Ni coating) Cu-1 wt.% GNPs-0.5 wt.% α-Al_2O_{3w}, (Ni coating) Cu-1.5 wt.% GNPs-0.5 wt.% α-Al_2O_{3w}, and samples were noted as CA1, CA2, CA3, CA4 for easy differentiation, and samples preparation flow chart is shown in fig. 1 below. The Cu powders and GNPs used in this study were provided by Shanghai Naiou Nano Technology Co., Ltd. α-Al_2O_{3w} were provided by Advanced Composites Research Department, Tsinghua Innovation Center, Dongguan, China, and chemical reagents were provided by Chengdu Kelong.

Table 1 Solution composition and parameters of electroless plating

	Main salt	Reducing agent	Complexant	pH regulator	pH
Cu coating	$CuSO_4 \cdot 5H_2O$	HCHO	$C_{10}H_{14}N_2Na_2O_8 \cdot 2H_2O$ $C_4H_4O_6KNa \cdot 4H_2O$	NaOH	12-13
Ni coating	$NiSO_4 \cdot 6H_2O$	$NaH_2PO_4 \cdot H_2O$	$Na_3C_6H_5O_7 \cdot 2H_2O$	$NH_3 \cdot H_2O$	10-11

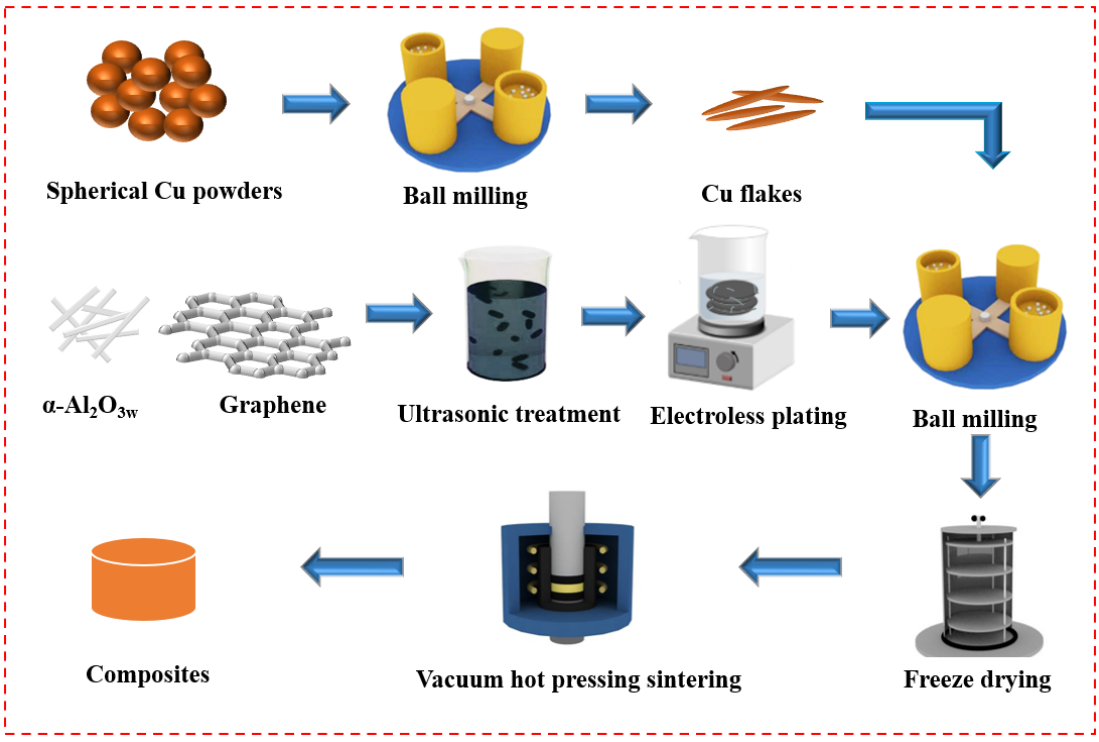

Fig. 1 Schematic diagram of the preparation of Cu-GNPs-α-Al_2O_{3w} laminated composites

2.2 Characterization of composites

The actual densities (ρ) of samples were determined using Archimedean drainage method and densities were calculated in conjunction with theoretical densities. A scanning electron microscope (ZEISS Gemini SEM 300) equipped with an energy dispersive X-ray spectroscopy (EDS) detector was used to analyze microstructure of powders and blocks. The specimens used in SEM were cut to a size of 5×5×5 mm^3 and then ground with various grit sizes of silicon carbide sandpaper and polished to 0.5 μm with a diamond paste. Also, for further characterization of interfacial microstructure, it was observed using a transmission electron microscope (TEM, JEM 2100F). X-ray instrument (x pert pro-mpd, Panalytical, Netherlands) was used to analyze phase composition of powders and bulk forms. To test the mechanical properties of composites, a universal testing

machine (WDW-3100) was used to measure tensile and compressive strength. The loading rate for tensile and compression tests was 0.5 mm/min. To further investigate the fracture and strengthening mechanisms of composites, SEM (ZEISS Gemini SEM 300)) and EDS were used to characterize and study fracture morphology of composites

3. Results and discussions

3.1Characterisation of reinforcement and composite powders

To improve interface contact, Cu\Ni-coated is introduced on the reinforcement surface by electroless plating. The schematic diagram of electroless plating is shown in fig. 2. The reinforcement is first ultrasonically roughened, and the rough surface increases the chance of metal ion deposition, thus improving the coating quality. Subsequently, sensitization caused Sn^{2+} to adsorb on the surface of reinforcement under acidic conditions. Subsequently, with addition of Pa^{2+}, Sn^{2+} acts as a reducing agent to reduce Pa^{2+} to Pd particles, thus forming an activation center on the surface of enhancer [34,39]. At the surface activation center, Cu is generated on the surface of reinforcement by reaction (1) [40]. In the process of electroless nickel plating, hypophosphite in electroless plating solution forms phosphite by catalytic dehydrogenation and also forms primary ecological hydrogen ions, as in reaction (2). The primary ecological hydrogen ion adsorbs and reduces the nickel ion in solution to nickel, which is deposited on the surface of the workpiece as reaction (3) [24,26,41] . It is worth noting that Ni deposited on the surface in turn plays a catalytic role in the subsequent reduction reaction [26,42]. As in reaction (4), this autocatalytic effect promotes the generation of subsequent Ni, resulting in a better Ni coating.

$$2HCHO + Cu^{2+} + 4OH^- \rightarrow Cu + 2HCOO^- + H_2 + 2H_2O \quad (1)$$

$$H_2PO_2^- + OH^- \rightarrow HPO_3^{2-} + H_2O + 2[H] \quad (2)$$

$$Ni^{2+} + 2[H] + 2OH^- \rightarrow Ni + 2H_2O \quad (3)$$

$$H_2PO_2^- + Ni^{2+} + 3OH^- \rightarrow Ni + HPO_3^{2-} + 2H_2O \quad (4)$$

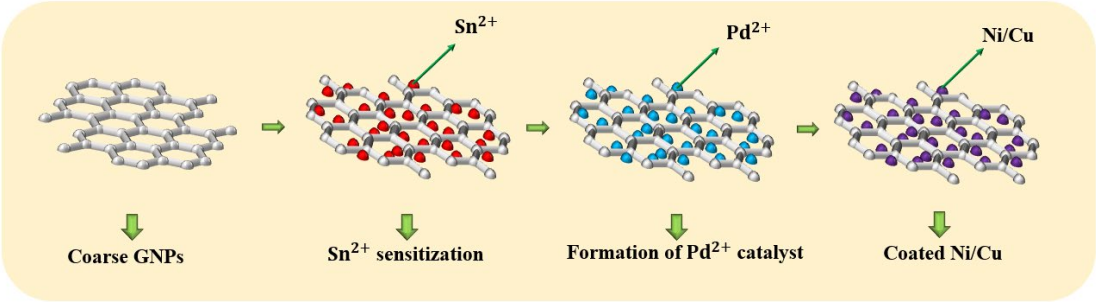

Fig. 2 Schematic diagram electroless plating process on the surface of GNPs

Fig. 3 shows surface morphology and EDS images of GNPs and α-Al_2O_{3w} after electroless plating. Since GNPs tend to curl, the flat GNPs are selected to observe surface coating as shown in fig. 3(a,b,e,f). The surface of GNPs is flat and smooth, and EDS results show that surface of GNPs after electroless plating is uniformly covered with Cu\Ni-coated. Fig. 3(c,d,g,h) shows that α-Al_2O_{3w} also obtained a surface coating of Cu\Ni after surface pretreatment. Comparing the results of different coating obtained, it is found that Ni coating on the surface of reinforcement is more uniform and thicker than Cu coating. This is due to the autocatalytic effect of Ni during electroless plating process, and Ni formed first has a promotion effect on the subsequent reaction, thus making Ni coating more uniform. Due to the autocatalytic effect of Ni, this phenomenon is common under the same experimental parameters. It is noteworthy that a small amount of Cu\Ni enrichment can be found on the α-Al_2O_{3w} surface. This may be due to special fiber structure of α-Al_2O_{3w}, the metal ions in solution are not easily deposited uniformly on the surface of α-Al_2O_{3w}, resulting in its enrichment in some strongly adsorbed areas. The two phases of metal coating on the reinforcement surface can increase wetting angle with matrix during the sintering process, bringing better interfacial bonding [17,26,43].

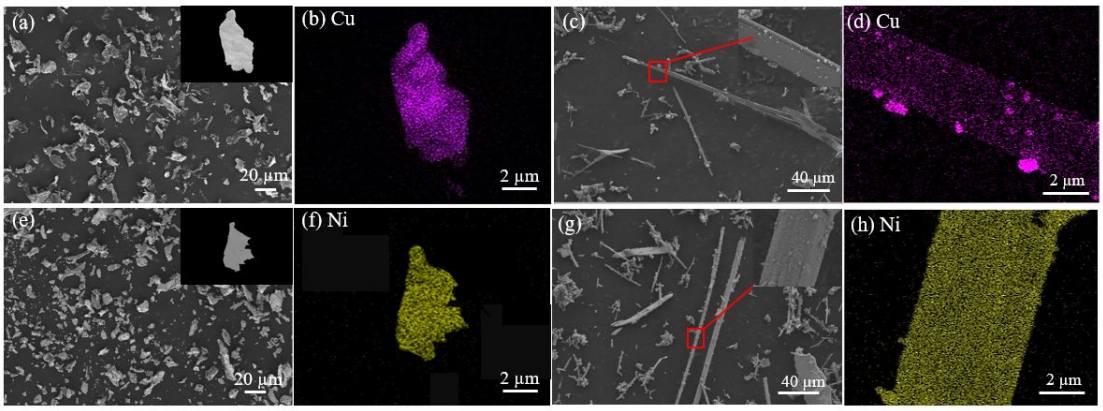

Fig. 3 (a) Microscopic morphology of Cu coating GNPs; (b) surface EDS of GNPs; (c) microscopic morphology of Cu coating α-Al_2O_{3w}; (d) surface EDS of α-Al_2O_{3w}; (e) microscopic morphology of Ni coating GNPs; (f)

surface EDS of GNPs; (g) microscopic morphology of Ni coating α-Al_2O_{3w}; (h) surface EDS of α-Al_2O_{3w}

The ball milling process exerts compressive and shearing forces on the powders through collision of the spheres, causing copper particles to undergo plastic deformation. With time, the spherical Cu powders gradually transforms into flakes. The Cu flakes with large aspect ratio have a larger contact area with reinforcement, which brings better interfacial bonding [35,44] . However, with the increase of ball milling time, the flake powders will be broken. The broken Cu flakes will form larger voids during sintering process, which will reduce the densities and agglomerate reinforcement. Therefore, ball milling time should be controlled to avoid excessive deformation of Cu flakes. According to preliminary work and experiments, a ball milling time of 6 h is appropriate [20]. Fig. 4 shows SEM and EDS images of composite powders. Fig. 4(a-d) shows that the size of Cu flakes is relatively uniform, roughly around 30 μm, andpresence of α-Al_2O_{3w} can be observed from it. However, GNPs cannot be clearly observed in fig. 4(a-d). In order to observe the coating on the surface of the reinforcement after mixing, Fig. 4(e-l) shows the elemental distribution on the surface of the reinforcement in mixed powder. Among them, Fig. 4(e-h) shows the Cu coating on the surface of GNPs and α-Al_2O_{3w}, and Fig. 4(i-l) shows the Ni coating on the surface of GNPs and α-Al_2O_{3w}. It was observed that coating on the surface of the reinforcement in mixed powder is well preserved, and there is no obvious destruction of the coating. Also, the deposition of Ni coating on the surface of GNPs and the roughness on the surface of α-Al_2O_{3w} are better than that of Cu coating, which is the same as the previous results. The EDS results show that Cu\Ni-coated is still present on the surface after powders mixing, which indicated that coating formed by electroless plating is well bonded to reinforcement a damage to coating by ball milling is small. The good adhesion of Cu\Ni-coated also allows good bonding between reinforcement and matrix during subsequent sintering process, thus improving interfacial bonding of composites.

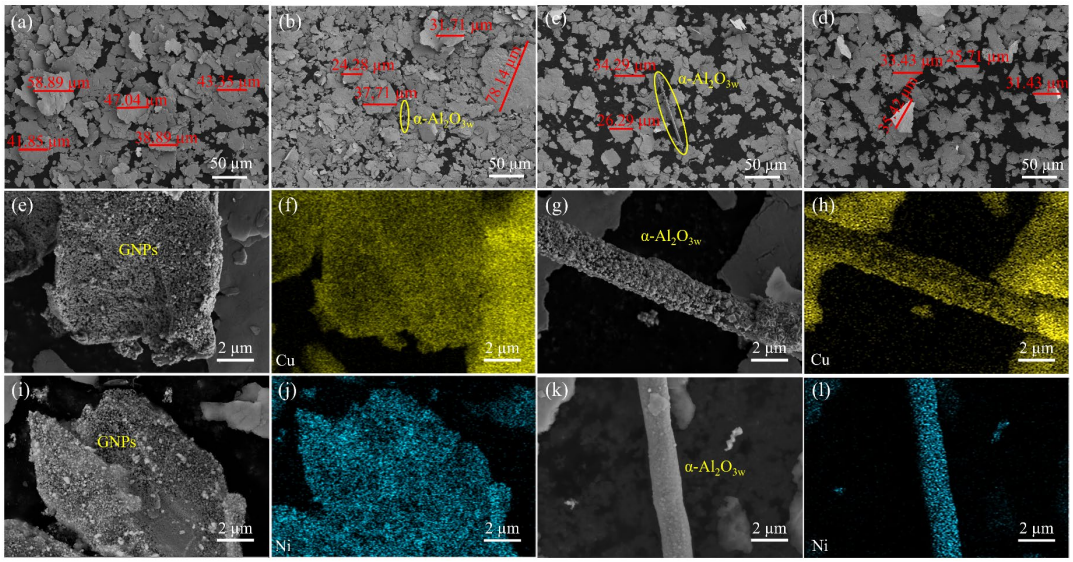

Fig. 4 SEM and EDS images of composite powders after 1 h of mixing (a) CA1; (b) CA2; (c) CA3; (d) CA4; (e,f) GNPs morphology and the distribution map of Cu; (g,h) α-Al_2O_{3w} morphology and the distribution map of Cu; (i,j) GNPs morphology and the distribution map of Ni; (k,l) α-Al_2O_{3w} morphology and the distribution map of Ni

Fig. 5 shows XRD pattern of Cu-GNPs-α-Al_2O_{3w} composite powders. The characteristic peak spectra of Cu (PDF # 70-3090) and GNPs (PDF # 71-3739) can be clearly seen in fig. 5, but the peaks of α-Al_2O_{3w} (PDF # 10-0173) are weak, while diffraction peaks of Ni are not detected. The reason for this phenomenon may be that the content of Ni is low and signal is blocked by Cu matrix. No oxides of Cu or other alloying elements are detected in XRD pattern, which indicates that no oxidation occurred during ball milling process. Choi et al. [45] investigated the grinding behavior of Cu particles during the preparation of CNTs-reinforced Cu matrix composites by high-energy ball milling. They found that the crystal structure of the powders sample did not change during the ball milling process and the raw material existed according to its own morphology by X-ray diffraction analysis, which is consistent with the results of this work.

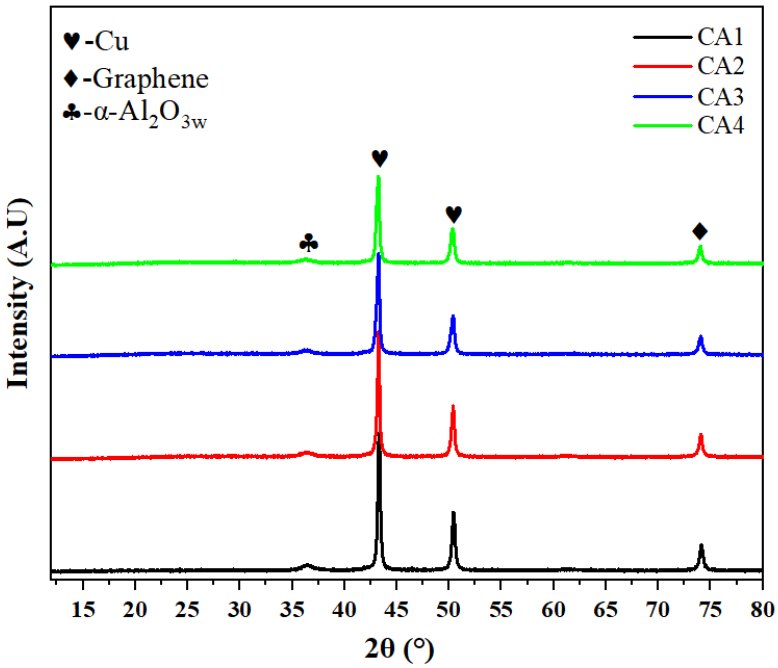

Fig. 5 XRD diagram of composite powders

3.2 Characterisation of composites

Fig. 6 shows SEM image of cross-section of composites block after sintering. It can be observed that reinforcement is uniformly distributed in matrix, and reinforcement appear to be regularly distributed in parallel. Observing fig. 6(a, b), it can be seen that at lower content of GNPs, reinforcement have a smaller size in the Y-direction, and overall trend of diffuse distribution is observed. All composites show laminated effect that is not obvious. Meanwhile the direction of α-Al_2O_{3w} dispersion may be in X or Y direction, but all are parallel to XY plane of laminated structure. In order to clarify the distribution of the reinforcement, EDS was performed on Fig. 6(c) to characterize elemental distributions, and the results are shown in Fig. 6(e-h). The C element corresponds to the distribution of GNPs, and Al and O elements correspond to the distribution of α-Al_2O_{3w}. The results show that the GNPs and α-Al_2O_{3w} show a clear laminated distribution in the XY plane, and the reinforcement do not appear to aggregate with each other. With the increase of GNPs content, the size of the reinforcement in Y-direction increases significantly and reinforcement laminated distribution is more obvious. In the sample with GNPs content of 1 wt.%, GNPs of larger size could be observed in field of view, while a large number of laminated distributions of reinforcement appeared in composites at GNPs content of 1.5 wt.%, when GNPs agglomeration

phenomenon is more obvious. Due to the two-dimensional structure of GNPs and α-$Al_2O_{3w,}$ they are geometrically compatible with Cu flakes, resulting in a regular laminated d distribution of the reinforcement in matrix. The reinforcement is regularly arranged in the XY plane, and the overall laminated structure of composites is more successful. However, in the case of excessive GNPs content, aggregation occurs due to the strong π-π bonding between GNPs [28,36]. The occurrence of agglomeration has a negative impact for properties of composites.

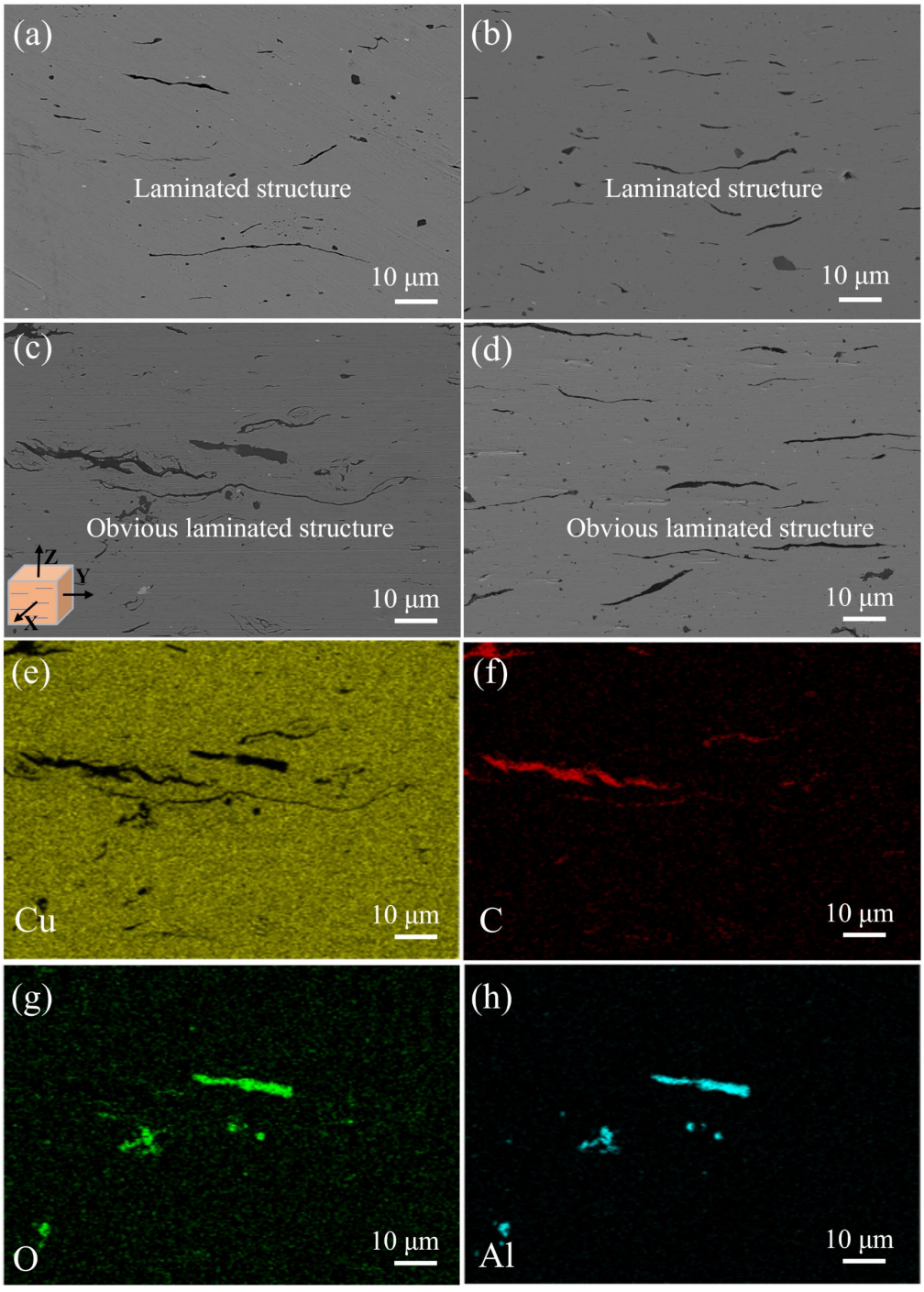

Fig. 6 SEM images of Cu\Ni-coated GNPs and α-Al_2O_{3w} reinforced laminated Cu matrix composites (a) CA1; (b)

CA2; (c) CA3; (d) CA4; (e) the distribution map of Cu; (f) C; (g) O; (h) Al

To determine the surface coating of composites after sintering, interfacial microstructure and element distribution of composites is performed as shown in fig. 7. The results show that no significant presence of coating can be observed at interface location. The Cu coating reinforcement do not suffer from elemental deficiency at the interface. But in fig. 7(b), it can be seen that α-Al_2O_{3w} \Cu interface exists again at the interstices, and interfacial bonding is poor. However, the GNPs with Ni coating and α-Al_2O_{3w} do not observe the presence of defects at interface position, and interface bonding between is better. At the same time, there is an obvious abrupt change in content of Ni elements, while no obvious Ni coating is observed in the microstructure. This may be due to the diffusion of Ni into Cu matrix during sintering process, resulting in detection of Ni in Cu matrix [26]. The diffusion of Ni coating into Cu matrix is also observed in study of Xu [26]. Diffusion occurs at the interface to form a stronger bond than original mechanical bond.

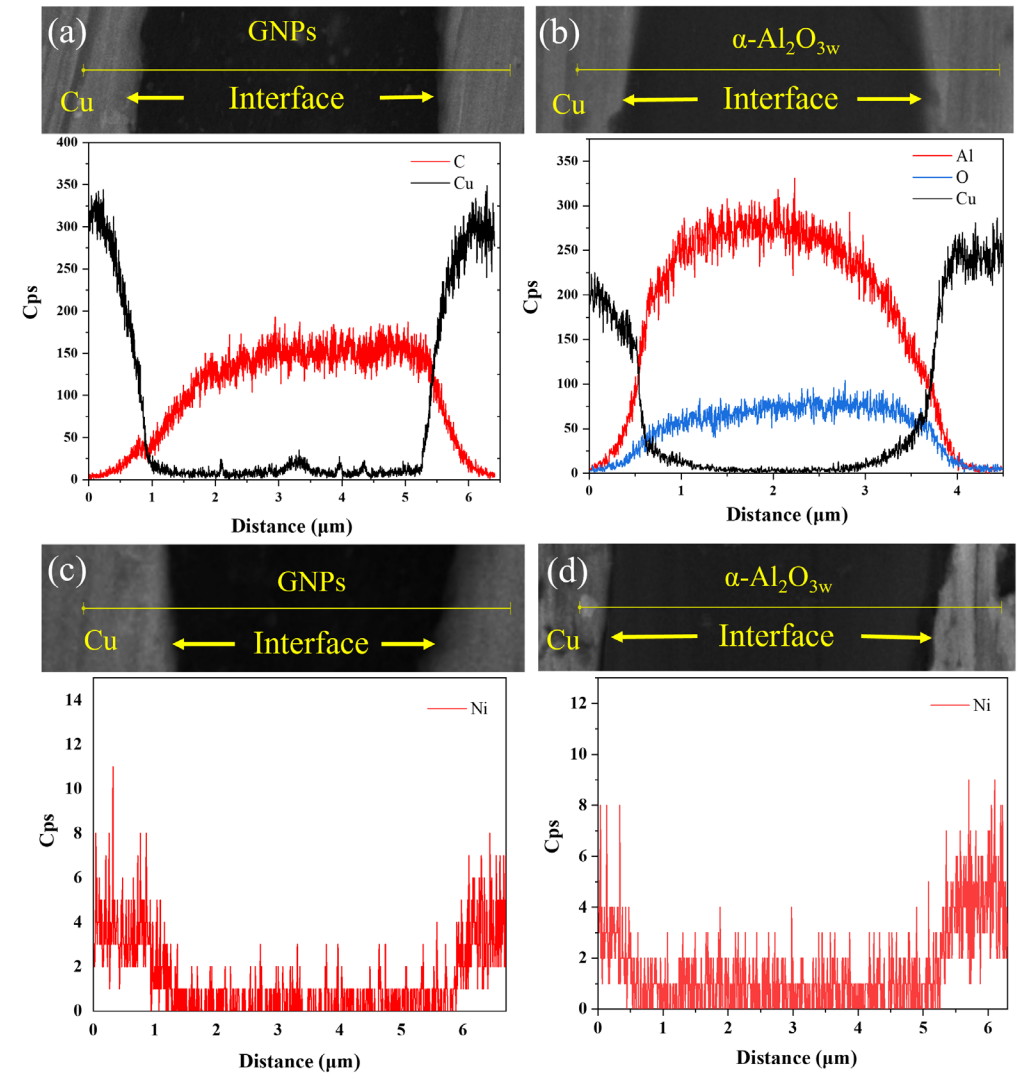

Fig. 7 (a) Cu coating GNPs; (b) Cu coating α-Al_2O_{3w}; (c) Ni coating GNPs; (d)Ni coating α-Al_2O_{3w} and Cu interfacial microstructure and element distribution

Fig. 8 shows XRD patterns of composites. Compared to fig. 5, the XRD pattern of composites shows the appearance of Ni peaks (PDF # 70-0989) in addition to the detection of same peaks as powders XRD results. After magnification of 40°-49° section, it is found that Ni peaks appeared in composites containing Ni coating. This is due to that Ni obtained by electroless plating is amorphous and transforms into face-centered cubic Ni crystals at high temperature thus appearing as Ni peaks in composites [28,46]. It is also found that the position of Cu peak is shifted to right compared to Cu coating on surface of reinforcement. The original data showed that Cu peaks of composites with Cu coating are 43.326° and 50.441°, while Cu peaks of composites with Ni coating are 43.959° and 51.083° corresponding to (111) and (200) crystallographic planes of Cu,

respectively. It proves that Cu characteristic peak is significantly right shifted. The Bragg's Law equation is used to analyze this phenomenon [21]:

$$d_{hkl} = \lambda/2sin\theta \tag{5}$$

According to Bragg's Law equation, an increase in θ is accompanied by a decrease in the crystal plane spacing d_{hkl} decreases. According Cu-Ni phase diagram [47] Cu-Ni can form solid solution at 650°C. The diffusion of Ni elements during the sintering process results in the formation of Cu-Ni solid solution in matrix. The formation of solid solution leads to the deformation of Cu lattice, so Cu peaks in XRD are shifted. The results show that no chemical reaction between reinforcement and matrix occurs during sintering process.

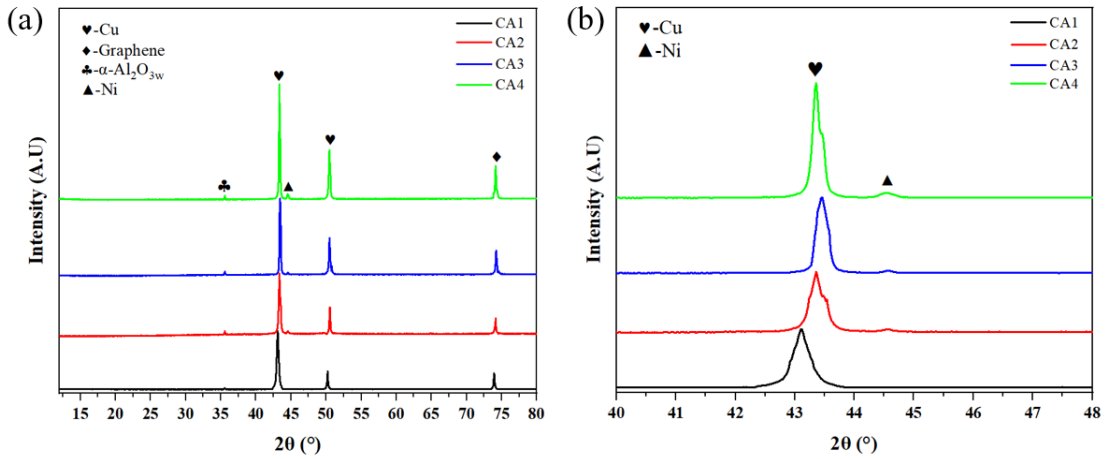

Fig. 8 (a) XRD of Cu\Ni-coated GNPs and α-Al_2O_{3w} reinforced laminated Cu matrix composites; (b) XRD local magnification

Fig. 9 is TEM results of CA1. Fig. 9(a) shows interface between Cu and GNPs. The results show that contact at Cu-GNPs interface is good, and interface between GNPs and matrix is continuous and clean. Fig. 9(b,c) HRTEM images of Cu-GNPs interface and the results of fast Fourier inverse transform (IFFT) for selected regions. The results show that Cu-GNPs interface is clearly distinguished and not chemically reacted, the interdiffusion between GNPs and Cu during sintering forms an interlocking effect [40]. Meanwhile, observation of IFFT results of Cu and GNPs reveals that crystal structure of Cu is better, with 0.182nm interplanar crystal spacing corresponding to Cu (200) crystal faces. In contrast, a large number of dislocations and dislocation rings were found in IFFT results of GNPs. This is due to thermodynamic mismatch between Cu and GNPs, and residual thermal stresses inside material after cooling, which leads to distortion of lattice structure

of GNPs at interface position [14,20]. Lattice deformation leads to reorganization of the crystal structure, so dislocations and dislocation loops appear in material. However, with deeper observation, voids appear at certain locations of the Cu-GNPs interface, as shown in Fig. 9(d). The generation of gaps is due to that lower sintering temperature results in weak diffusion dynamics during the sintering process, leading to an increase in the resistance of material densification process. The TEM results show that the Cu coating reinforcement improves the wettability between reinforcement and matrix during the sintering process, resulting in a better interfacial bond. However, due to the low sintering temperature and insufficient diffusion power during sintering, defects can be formed at certain locations on the interface. Such defects can have a significant negative impact on the mechanical properties of material.

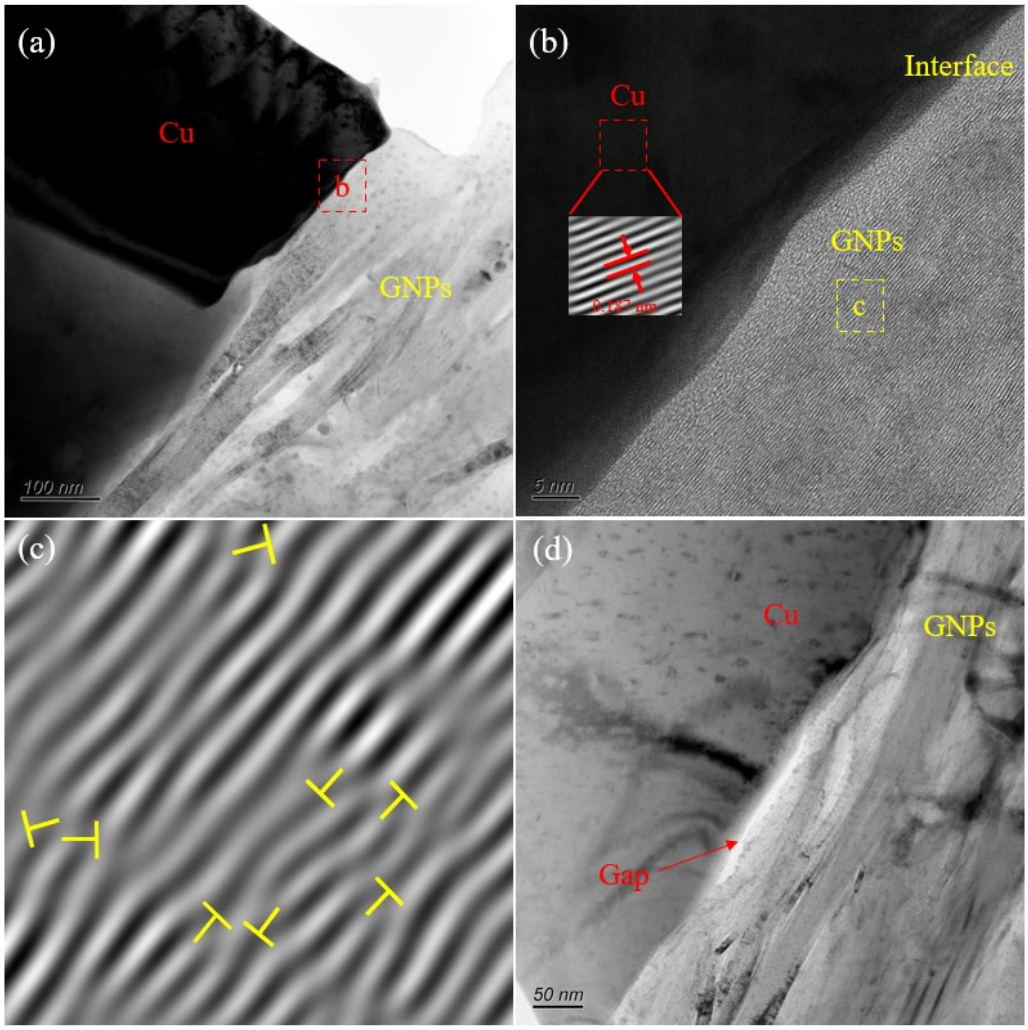

Fig. 9 TEM images of Cu coating GNPs and α-Al_2O_{3w} reinforced Cu matrix composites: (a) interface morphology of Cu and GNPs; (b) HRTEM of Cu-GNPs; (c) IFFT image of GNPs; (d) interface gap of Cu and GNPs

Fig. 10 shows the TEM images of Ni coating GNPs and α-Al_2O_{3w} reinforced laminated Cu matrix composites. A more pronounced laminated structure of matrix and laminated distribution of the GNPs is found in fig. 10(a,b). This suggests that the desired laminated structure can be achieved by combining FPM and vacuum hot pressing sintering. The reason why laminated structure is achieved can be explained by the fact that two-dimensional structure of GNPs and fibrous structure of α-Al_2O_{3w} do not cause damage to laminated Cu powders during mixing and sintering. The interdiffusion between Cu flakes during sintering causes the adjacent Cu flakes to stick together while encapsulating reinforcement between Cu flakes. The flake Cu powders acts as the soft phase and reinforcement acts as hard phase, forming a connection structure similar to mineral bridge in the pearl shell structure [20,31,34] thus forming laminated structure. This connection structure is the key to transfer the load from matrix to reinforcement. Fig. 10(b,c) shows the views of GNPs and α-Al_2O_{3w} in matrix. It is observed that reinforcement is tightly bound to matrix and no voids appear at interface. To explore the distribution of Ni elements in the material, fig. 10(d-f) shows the elemental distribution of fig. 10(b). It can be found that there is a small amount of Ni element in the Cu matrix around the GNPs. According to the Cu-Ni phase diagram, the reaction between Cu and Ni does not occur below 650°C to form a second phase, but exists in form of solid solution. They're infinitely miscible [46]. Ni diffuses into the Cu lattice to replace Cu atoms, thus forming a substitutional solid solution. The presence of solid solution brings solid solution strengthening, thus bringing higher strength to composites. At the same time, the amorphous Ni in coating diffuses into Cu matrix during sintering process. The highly chemically active Ni during the diffusion process provides impetus for the nucleation of Cu, thus promoting the densification process of composites [26,46]. Fig. 10(g) shows the HRTEM images between the GNPs and matrix, fig. 10(g) shows the IFFT results of selected regions. Fig. 10(g) shows that interface between GNPs and matrix is obvious, continuous and clean with good contact. Since no chemical reaction occurs between copper and GNPs, they form a mechanical interlocking effect to achieve a good mechanical bond [7,13]. Meanwhile, a small number of dislocations appear in GNPs, which is the same as results shown in fig. 9. Observing the IFFT results of matrix, it is found that there are obvious dislocations and dislocation rings in matrix, and Cu matrix shows relatively obvious lattice distortion. This is related to diffusion and solid solution strengthening effect of Ni. Comparing fig. 9(f), it can be determined that the diffusion phenomenon of Ni in coating caused the lattice distortion in matrix. Fig. 10(i)

shows the HRTEM images between α-Al_2O_{3w} and Cu. The results show that the lattice stripe spacing is 0.184 nm in the Cu region and 0.175 nm in the α-Al_2O_{3w} region. Interface zone is found in the HRTEM image. The interface zone is also found in Tan's study[11]. Due to difficult chemical reaction between α-Al_2O_{3w} and Cu [48], so the possibility of the interface layer being a compound is excluded. It is assumed that interface zone is formed during the sintering process. The α-Al_2O_{3w} surface also provides a large number of non-uniform nucleation sites for matrix when diffusion of Ni into matrix ends. During sintering Cu nucleates in large quantities on α-Al_2O_{3w} surface, while the lower sintering temperature results in slower grain growth and the formation of a nanoscale Cu layer on α-Al_2O_{3w} surface. The formation of interfacial layer can further improve the interfacial strength between α-Al_2O_{3w} and matrix, it can improve the efficiency of α-Al_2O_{3w} in transferring the load.

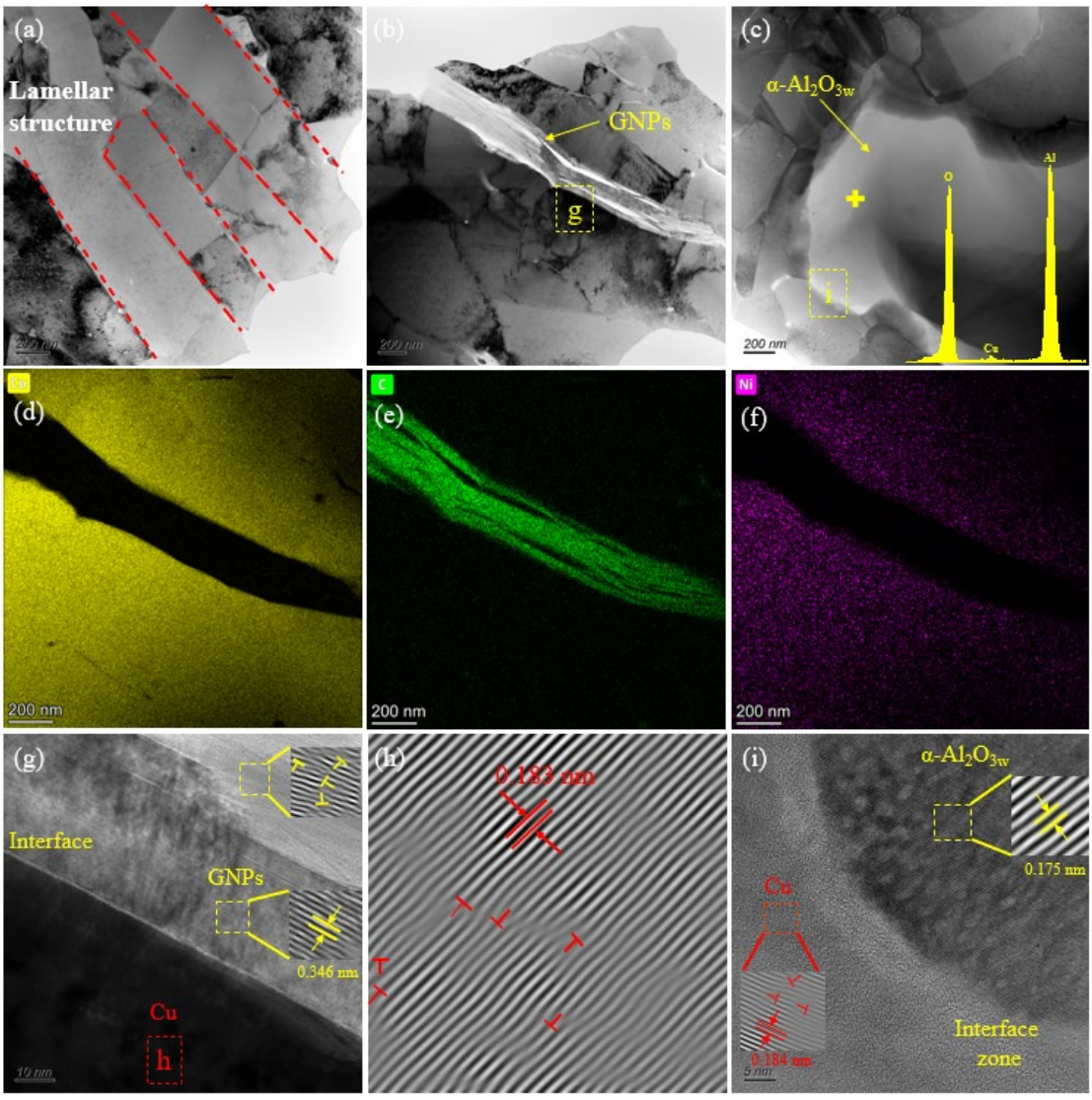

Fig. 10 TEM images of Ni coating GNPs and α-Al_2O_{3w} reinforced laminated Cu matrix composites: (a) laminated

structure; (b) GNPs; (c) α-Al_2O_{3w}; (d) Cu elemental distribution; (e) C elemental distribution; (f) Ni elemental distribution; (g) HRTEM images of the interface of Cu and GNPs; (h) IFFT image of Cu; (i) HRTEM images of the interface of Cu and α-Al_2O_{3w}

3.3 Mechanical properties analysis of composites

Table 2 shows the density and mechanical property parameters of composites. The results show that the densities of CA1 are significantly lower than other composites. Due to low sintering driving force of CA1 at low sintering temperature, it is difficult for powders sintering neck to fill voids during the sintering process, resulting in decrease in density. In contrast, Ni coating exists in amorphous state on surface of reinforcement, and amorphous Ni has high activity to reduce diffusion activation energy [46]. Meanwhile, during sintering process, good geometrical compatibility between Cu flakes and reinforcement provided more diffusion paths for Ni migration and promoted sinter densification [49]. Similarly, in the study of Xu [26], it is found that addition of Ni coating could reduce densification temperature range of composites. However, as the content of GNPs increases, the agglomeration of reinforcement also hinders densification process, leading to a decrease in densification. The decrease in composites densification leads to cracks at internal defect locations, resulting in premature failure of composites. Fig. 11 shows composites tensile-strain and compression-strain curves. Combined with the data in Table 2, composites tensile and compressive properties show same trend. The mechanical properties of composites with Ni coating showed a greater improvement than those of the Cu coating samples for same reinforcement content. For Cu coating composites, the interfacial gap between reinforcement and matrix becomes a crack initiation site due to low dense material. The addition of Ni coating promotes the densification of the material, while Ni and Cu matrix will form solid solution to bring solid solution strengthening effect. At the same time, the tensile and compressive strength of the material increases and then decreases with the increase of GNPs content. According to previous study [13], the presence of GNPs can prevent crack from expanding when crack appears at the position of α-Al_2O_{3w} , thus it can enhance the strengthening effect of α-Al_2O_{3w}. With the increase of GNPs content, hybridization enhancement effect becomes more and more obvious. Tensile strength of composites reaches 336.12 MPa and compressive strength is 448.81 MPa when the content of GNPs is 1 wt.%. However, with the

increase of GNPs content, strong van der Waals forces between GNPs lead to generation of clusters. The GNPs at the cluster position cannot play strengthening role well and often become defective position in composites [14,36]. The agglomeration location of reinforcement often becomes a defect location in composites, leading to a decrease in mechanical properties. As graphene content continued to increase, the mechanical properties decreased, which is mainly due to the increase of internal defects caused by the appearance of agglomeration. The results show that Ni coating GNPs and α-Al_2O_{3w} reinforced laminated Cu matrix composites have high densities and high mechanical properties. However, too much graphene can also increase internal defects leading to a loss of strength.

Table 2 Mechanical properties of Cu\Ni-coated GNPs and α-Al_2O_{3w} laminated copper matrix composites

Samples	Density (%)	Tensile strength (MPa)	±Error (MPa)	Elongation (%)	Compression strength (MPa) (50% strain)	±Error (MPa)
CA1	93.97±0.18	191.08	±2.43	11.33	367.33	±2.49
CA2	98.46±0.11	312.33	±4.43	18.62	412.43	±4.17
CA3	98.91±0.09	333.65	±3.46	16.32	448.81	±3.94
CA4	97.69±0.15	309.25	±5.04	15.02	404.92	±3.85

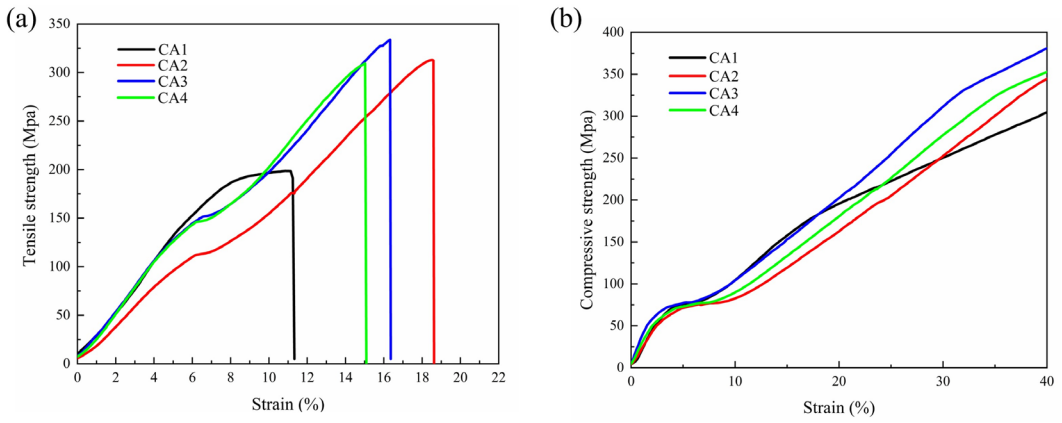

Fig. 11 Cu-GNPs-α-Al_2O_{3w} laminated composites: (a) Tensile stress-strain curve; (b) Compressive stress-strain curve

Fig. 12 shows comparative tensile/compression properties of laminated Cu-GNPs-α-Al_2O_{3w} composites. Since there are fewer studies on GNPs and α-Al_2O_{3w} hybridized reinforced

Cu matrix composites, the comparison of other studies related to GNPs and α-Al_2O_{3w} in fig. 12 [2,5,9,11,13,14,28,50,51]. The comparative results show that tensile process of composites in this experiment obtains high strength while maintaining good elongation, composites obtaining good balance between strength and toughness. Also in compression experiments, the laminated composites do not fracture even at 50% strain, while composites under other related systems all showed fracture, while overall compression strength reached high level. The comparison results show that laminated Cu-GNPs-α-Al_2O_{3w} composites prepared by electroless plating and FPM methods achieve a balance of high strength and toughness. The presence of the coating increases bond at interface location and enhances reinforcing effect of reinforcement. At the same time, the multiscale toughening mechanism of laminated structure ensures that composites maintain high toughness while obtaining high strength, and overall performance of composites is improved more significantly.

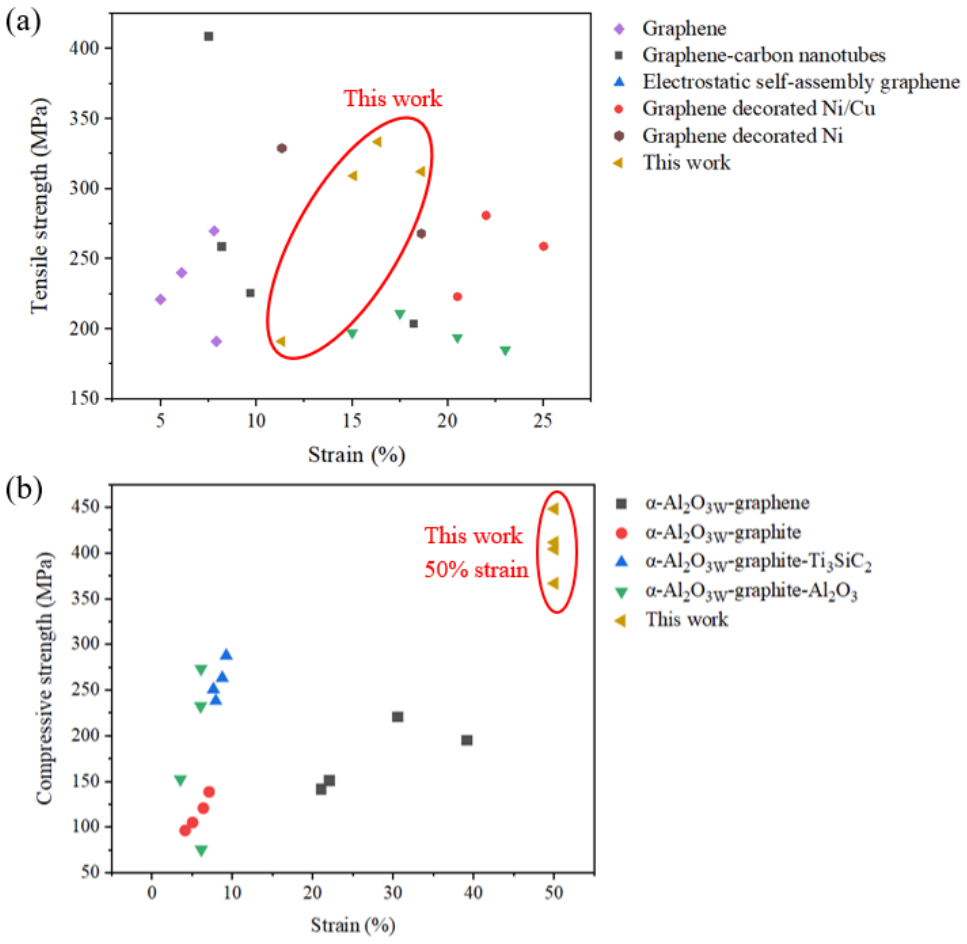

Fig. 12 Comparison of (a) tensile strength and elongation; (b) compressive strength and strain of this work with related literature [2,5,9,11,13,14,28,50,51]

3.4 Fracture analysis of composites

Fig. 13 shows the tensile fracture diagram of composites. The results show that all composites have obvious tough nests and all show ductile fracture. At the macroscopic level sample fractures show a clear laminated structure. Also, in fig. 13, it can be observed that α-Al_2O_{3w} shows both pullout and fracture. Two failure modes of whisker during load transfer can effectively consume energy required for crack expansion [5,52] and thus achieve purpose of strengthening. In order to investigate the effect of laminated fracture on composites properties, the local area of fracture is studied in a magnified manner. In fig. 13(b), there are obvious pores around GNPs, which are caused by defects at interface due to poor bonding of interfaces, and thus generated during the tensile process. The presence of pores greatly reduces mechanical properties of composites. However, the structure is much tighter in composites with Ni coating. The magnified fractures exhibit more pronounced laminated structure and GNPs show a regular parallel distribution. Parallel distribution of GNPs showed signs of pull-out and α-Al_2O_{3w} fracture was observed. The pull-out and fracture of multiple reinforcement is main reasons for the strengthening obtained in matrix. In addition, fractures of all composites exhibited a distinct laminated structure and the tough nests tended to be flat in shape. The laminated structure excites intra-layer interlocking in GNPs/Cu composites [20,31]. Due to interlocking, Cu matrix is continuous throughout composites, which facilitates exploitation of inherent plasticity of matrix. Microcracks develop into large cracks in the direction of laminate and are deflected between laminates. The process of crack extension and crack deflection also leads to effective energy dissipation, which facilitates the toughening of composites [37,38]. However, with the increase of GNPs content, pores by GNPs agglomeration are found in composites with GNPs content of 1.5 wt.%. The presence of pores reduces the load transfer capability of GNPs, while the crack expansion is accelerated at interfacial location, causing premature composites failure.

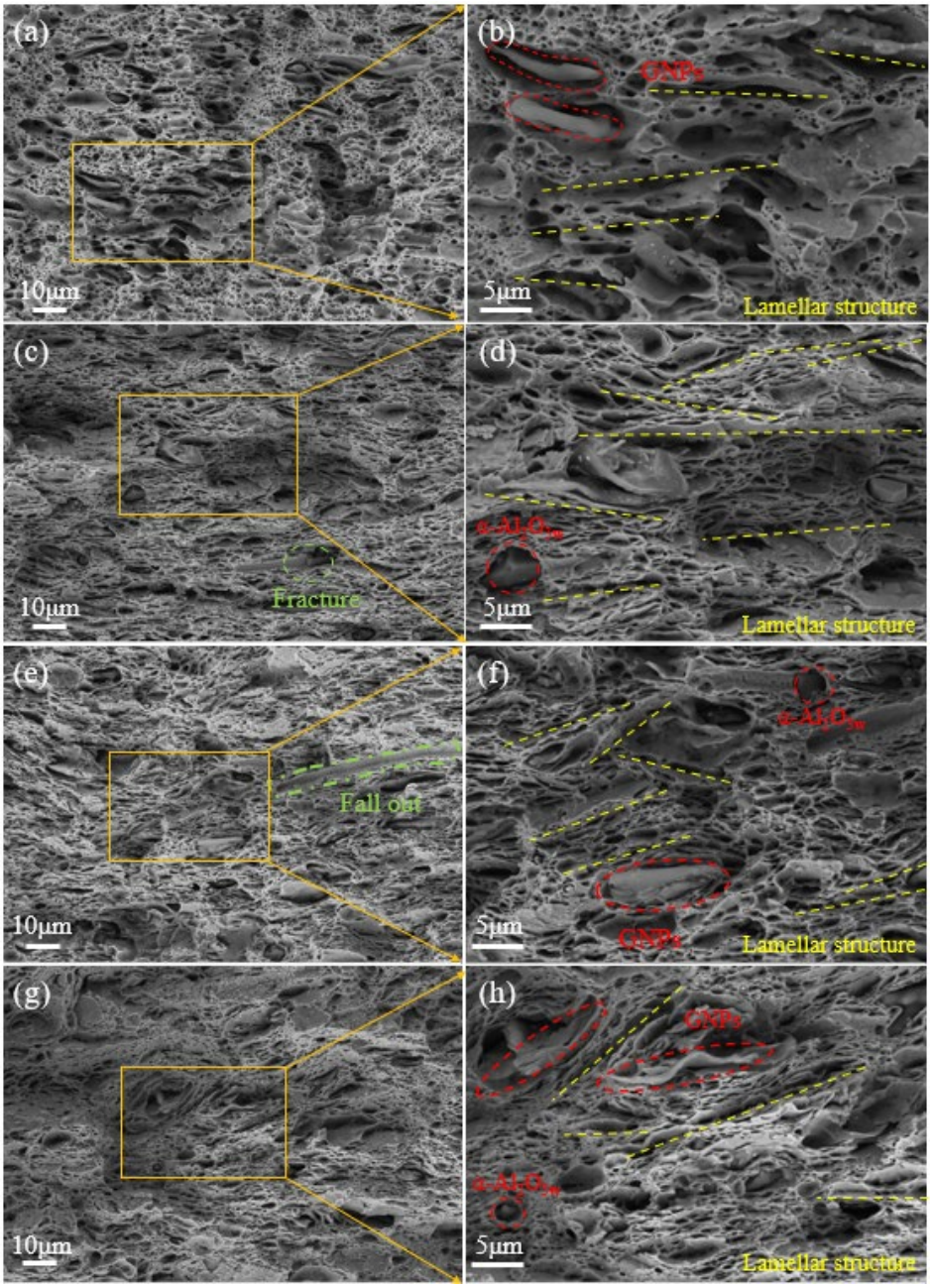

Fig. 13 Microscopic morphology of tensile fracture of composites (a,b) CA1; (c,d) CA2; (e,f) CA3; (g,h) CA4

Discussion

The strengthening mechanisms of Cu\Ni-coated GNPs and α-Al_2O_{3w} reinforced laminated Cu matrix composites are mainly load transfer, solid solution strengthening and second phase strengthening. When composites are subjected to an external force, part of load is transferred from matrix to reinforcement to provide strengthening effect. The efficiency of load transfer at interface

affects the overall strength of composites [4,52]. It is assumed that interfacial strength is higher than yield shear strength of Cu (τ_m). The increase in yield strength of GNPs and α-Al_2O_{3w} reinforced laminated Cu matrix composites caused by load transfer ($\Delta\sigma_{LT}$) can be calculated theoretically based on the shear hysteresis model as shown in equation (6) [53,54].

$$\Delta\sigma_{LT} = \alpha V_{r1}\sigma_{r1} + \alpha V_{r2}\sigma_{r2} - V_r\sigma_m \quad (6)$$

Where V_{r1}, V_{r2} are the volume fractions of GNPs, α-Al_2O_{3w}, respectively σ_{r1}, σ_{r2} and σ_m are the strengths of GNPs, α-Al_2O_{3w} and Cu, respectively. The coefficient α is related to aspect ratio τ_m and σ_r is related and can be expressed as $\alpha = (\tau_m s) / (2\sigma_r)$. Therefore, the $\Delta\sigma_{LT}$ can be expressed by equation (7).

$$\Delta\sigma_{LT} = \frac{1}{2}\tau_{m1}s_1V_{r1} + \frac{1}{2}\tau_{m2}s_2V_{r2} - V_r\sigma_m \quad (7)$$

From equation (6), it can be seen that the effect of load transfer mechanism is mainly determined by length-to-diameter ratio s determines. Since both GNPs and α-Al_2O_{3w} have large aspect ratios, both have prominent load transfer effects in composites. The fracture shows that fracture surface shows a typical step-like fracture parallel to each layer, and there are also fragments of GNPs on fracture step, indicating that interlaced GNPs play an obstructive and deflective role on fracture. In contrast, the fibrous α-Al_2O_{3w} shows both pull-out and fracture, the different failure modes can effectively consume the energy required for crack expansion and better exert strengthening effect [9,12]. However, the shear hysteresis model only considers the aspect ratio in the actual optimized interconnected structure also helps to improve the strength of composites. Recent experiments have shown that when cracks appear at the interface between α-Al_2O_{3w} and matrix, GNPs with large aspect ratios can block the crack expansion path and thus achieve the effect of hybridization enhancement [13]. The synergistic effect can achieve the strengthening effect of "1+1>2". Meanwhile, strengthening and toughening effect of reinforcement depends on its failure mode due to the presence of laminated structure. In the shear hysteresis model, critical aspect ratio of reinforcement (S_c) determines damage mode of load transferred from shear stress generated in matrix to reinforcement [29,31], S_c can be expressed as follows:

$$S_C = \sigma_p/\tau_y \quad (8)$$

σ_p is strength of reinforcement, and τ_y is strength of Cu. When actual aspect ratio of reinforcement is greater than critical value ($S>S_C$), composites break in fracture mode of

reinforcement, indicating that composites is brittle. In the case of $S < S_C$, reinforcement consume part of the energy required for crack expansion when it is pulled out and reinforcement fails in a high toughness pull-out mode. Taking the above conclusions together, the fracture mechanism diagram of composites is shown in fig. 14. Due to the presence of laminated structure, the larger grain size in plane facilitates dislocation movement, while interlayer interface and nanocrystals hinder dislocation movement perpendicular to plane direction. Stress concentration occurs when dislocations are inserted in a certain plane. In this case, the direction of crack movement is deflected, thus improving the stress concentration in plane [21,38,55]. The crack deflection inhibits occurrence of local strains in composites, allowing the energy to be better expended in crack expansion process. The overall crack path is extended so that higher energy is required to fracture composites, thereby increasing composites strength and toughness [20,37]. Accordingly, the crack extension path of the laminated composites appears as a step-like pattern in fig. 14. In addition, due to two-dimensional structure and large aspect ratio of GNPs and α-Al_2O_{3w} [5,13,27], it makes both of them not only help to complete the construction of laminated structure, but better laminated structure makes composites obtain better toughness. The presence of laminated structure makes cracks show multi-directional deflection, but due to low sintering temperature, composites with Cu coating is shown in transmission results to produce significant defects at interface. When crack extends to interfacial gap, due to poor interfacial bonding, cracks mutate at the defect location, leading to premature material failure， as shown in fig. 14(a). In contrast, the addition of Ni coating promotes composites densification process and improves interfacial bonding between matrix and reinforcement, as in fig. 14(b). Meanwhile, Ni diffuses into matrix during sintering process to form microalloying effect, and solid solution strengthening phenomenon of Ni in matrix hinders movement of dislocations and enhances strength of matrix. In summary, the introduction of Ni coating improves interfacial bonding of composites and brings about solid solution strengthening, which combined with building of laminated structure results in high strength and good toughness of composites.

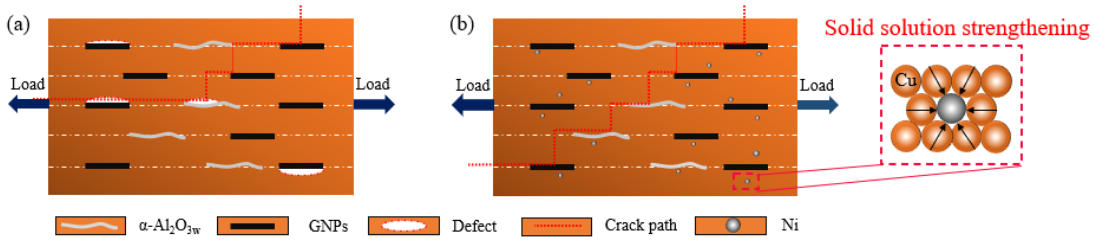

Fig. 14 (a) Cu coating; (b) Ni coating GNPs and α-Al_2O_{3w} reinforced laminated Cu matrix composites strengthening and fracture mechanisms

Conclusion

In this study, GNPs-α-Al_2O_{3w} reinforced laminated Cu matrix composites with Cu\Ni-coated were successfully prepared by combination of two methods: FPM and vacuum hot-press sintering. The effects of Cu\Ni-coated and laminated structure on the microstructure, interfacial bonding effect and mechanical properties were discussed. The main conclusions are as follows:

1. Cu\Ni-coated is successfully introduced to GNPs and α-Al_2O_{3w} surfaces by surface pretreatment and electroless plating, and relatively uniform coating is obtained. Subsequently coating is not significantly damaged during ball milling process. Finally, Cu-GNPs-α-Al_2O_{3w} laminated composites are successfully prepared by vacuum hot pressing sintering.
2. The TEM results show that laminated structure was successfully built. Due to low sintering temperature, composites which reinforcement with Cu coating show significant gap at interface. However, the incorporation of Ni coating provides impetus for nucleation of composites during sintering process, so that tight bond is obtained at interface. GNPs are tightly bonded to matrix and interfacial bond is mechanical. The diffusion layer appears at interface between α-Al_2O_{3w} and Cu. Two bonding methods improve interfacial strength and facilitate the load transfer. Moreover, Ni forms a solid solution with matrix, which creates solid solution strengthening effect in matrix.
3. Composites with Cu coating have weaker interfacial bonding with matrix, resulting in lower densities and mechanical properties than composites with Ni coating. As the content of GNPs increases, tensile and compressive strengths of composites tend to increase and then decrease, while elongation is always maintained at relatively high level. When GNPs content is 1 wt.%, tensile strength reached 336.12 MPa and compressive strength at 50% strain reached 448.81 MPa. With increase of GNPs, GNPs show agglomeration, leading to decrease in density and mechanical properties of composites.
4. The fractures all have distinct laminated structure. During fracture process, α-Al_2O_{3w} and

GNPs with different aspect ratios play a reinforcing effect through failure modes of drawing and fracture for better strengthening. And the presence of laminated structure allows crack to be deflected, which results in multi-planar and multi-angle crack extension. The crack deflection effectively avoids stress concentration and prolongs crack extension path, which increases energy consumption during fracture, thus achieving a balance between strength and toughness of composites.

Declaration of competing interest

The authors declare that they have no known competing financial interests or personal relationships that could have appeared to influence the work reported in this paper.

Acknowledgements

This work was supported by Key Laboratory of Infrared Imaging Materials and Detectors, Shanghai Institute of Technical Physics, Chinese Academy of Sciences (No. IIMDKFJJ-21-10) and China Postdoctoral Science Foundation (No. 2018T110993). We would like to thank Analytical and Testing Center of Southwest Jiaotong University for partial testing.

Data Availability statement

The data used to support the findings of this study are available from the corresponding author upon request.

References

[1] Z. Balalan, F. Gulan, Microstructure and mechanical properties of Cu-B_4C and CuAl-B_4C composites produced by hot pressing, Rare Metals. 38 (2019) 1169-1177. https://doi.org/10.1007/s12598-019-01287-2

[2] J. Naseri, K. Ranjbar, M. Reihanian, Optimizing the strength and electrical conductivity of graphene reinforced Cu-Cr-Zr alloy fabricated by powder metallurgy and spark plasma sintering, Mater. Chem. Phys. 300 (2023) 127524.

https://doi.org/10.1016/j.matchemphys.2023.127524

[3] A. Jamwal, P.P. Seth, D. Kumar, R. Agrawal, K.K. Sadasivuni, P. Gupta, Microstructural, tribological and compression behaviour of copper matrix reinforced with Graphite-SiC hybrid composites, Mater. Chem. Phys. 251 (2020) 123090. https://doi.org/ 10.1016/j.matchemphys.2020.123090

[4] X.Y. Wen, R. Joshi, 2D materials-based metal matrix composites, J. Phys. D-Appl. Phys. 53 (42) (2020) 423001. https://doi.org/10.1088/1361-6463/ab9b5d

[5] G.H. Zhang, X.S. Jiang, Z.Y. Shao, H.L. Sun, Q. Ma, Z.P. Luo, Microstructures and mechanical properties of alumina whisker reinforced copper matrix composites prepared by hot-pressing and hot isostatic pressing, Mater. Res. Express. 6 (11) (2019) 116513. https://doi.org/ 10.1088/2053-1591/ab43eb

[6] W.J. Li, Y. Liu, G.H. Wu, Preparation of graphite flakes/Al with preferred orientation and high thermal conductivity by squeeze casting, Carbon. 95 (2015) 545-551. https://doi.org/ 10.1016/j.carbon.2015.08.063

[7] J.Q. Wang, W.N. Lei, Z.M. Xue, H.F. Qian, W.Q., Liu, Research progress on synthesis and application of graphene reinforced metal matrix composites, Cailiao Gongcheng. 46 (12) (2019) 18-27. https://doi.org/10.11868/j.issn.1001-4381.2017.001534

[8] A.K. Kasar, G. Xiong, P.L. Menezes, Graphene-reinforced metal and polymer matrix composites, Jom. 70 (6) (2018) 829-836. https://doi.org/10.1007/s11837- 018-2823-2

[9] G.H. Zhang, X.S. Jiang, C.J. Qiao, Z.Y. Shao, D.G. Zhu, M.H. Zhu, Investigation of the microstructure and mechanical properties of copper-graphite composites reinforced with single-crystal-Al_2O_3 fibres by hot isostatic pressing, Materials. 11 (6) (2018) 982. https://doi.org/10.3390/ma11060982

[10] P.C. Yu, R.J. Yang, Y.T. Chang, F.S. Yen, Fabrication of nano-scaled alpha-Al_2O_3 crystallites through heterogeneous precipitation of boehmite in a well dispersed theta-Al_2O_3-suspension, J. Am. Ceram. Soc. 90 (8) (2007) 2340-2346. https://doi.org/10.1111/j.1551-2916.2007.01746.x

[11] W.Y. Tan, X.S. Jiang, Z.Y. Shao, H.L. Sun, T.F. Song, Z.P. Luo, Fabrication and mechanical properties of alpha-Al_2O_3 whisker reinforced cu-graphite matrix composites, Powders Technol. 375 (2020) 124-135. https://doi.org/10.1016/j.powtec.2020.07.105

[12] Y. Zhong, H. Chen, W. Hu, G. Gottstein, Fiber damage and high temperature tensile properties of Al_2O_3 fiber reinforced NiAl-matrix composites with and without hBN-interlayer, Mat. Sci. Eng. A 464 (1-2) (2007) 241-248. https://doi.org/10.1016/j.msea.2007.02.072

[13] Z.Y. Shao, H.K. Pan, R. Shu, X.S. Jiang, M.H. Zhu, Microstructures and interfacial interactions of Al_2O_3 whiskers and graphene nano-platelets co-reinforced copper matrix composites, T. Nonferr. Metal. Soc. 32 (9) (2022) 2935-2947. https://doi.org/10.1016/S1003-6326(22)65994-6

[14] J. Wang, L.N. Guo, W.M. Lin, J. Chen, S. Zhang, S.D. Chen, The effects of graphene content on the corrosion resistance, and electrical, thermal and mechanical properties of graphene/copper composites, New Carbon Mater. 34 (2) (2019) 161-169. https://doi.org/10.1016/j.carbon.2019.04.095

[15] G. Singh, N. Sharma, S. Goyal, R.C. Sharma, Comparative measurements of physical and mechanical properties of AA6082 based composites reinforced with B_4C and SiC particulates produced via stir casting, Met. Mater. Int. 27 (11) (2020) 333-345. https://doi.org/10.1007/s12540-020-00666-0

[16] H. Bai, C. Xue, J.L. Lyu, Li J, G.X. Chen, J.H. Yu, Thermal conductivity and mechanical properties of flake graphite/copper composite with a boron carbide- boron nano-layer on graphite surface, Compos. Part A-Appl. Sci. Manuf. 106 (2018) 42-51. https://doi.org/10.1016/j.compositesa.2017.11.019

[17] Y. Huang, Y.S. Su, X.W. Guo, Q. Guo, Q.B. Ouyang, G.D. Zhang, Fabrication and thermal conductivity of copper coated graphite film/aluminum composites for effective thermal management, J. Alloy Compd. 711 (2017) 22-30. https://doi.org/10.1016/j.jallcom.2017.03.233

[18] X.H. Chen, P.Z. Liu, P. Liu, H.H. Chen, Preparation of copper-graphene layered composites by spark plasma sintering, Mater. Sci. Tech-Lond, 34 (14) (2018) 1693-1699. https://doi.org/10.1080/02670836.2018.1472908

[19] X.Z. Wang, Y.S. Su, Q.B. Ouyang, C.N. Zhu, H. Cao, D. Zhang, Fabrication, mechanical and thermal properties of copper coated graphite films reinforced copper matrix laminated composites via ultrasonic-assisted electroless coating and vacuum hot-pressing sintering, Mat. Sci. Eng. A 824 (2021) 141768. https://doi.org/10.1016/j.msea.2021.141768

[20] F. Luo, X.S. Jiang, H.L. Sun, J.Y. Shang, Y.L. Zhang, R. Shu, Mechanical and thermal properties of Cu-coated diamond reinforced Cu matrix bioinspired laminated composites, J. Alloy Compd. 938 (2022) 168584. https://doi.org/10.1016/j.jallcom.2022.168584

[21] Y.N. Tian, Z.H. Dou, L. Niu, T.A. Zhang, Studies on copper-coated boron carbide particle-reinforced copper-matrix/graphite self-lubricating composite materials, Russ. J. of Non. Ferr. Met+. 60 (5) (2019) 575-582. https://doi.org/10.3103/S106782121905016X

[22] J.H. Nie, C.C. Jia, X. Jia, Y. Li, Y.F. Zhang, X.B. Liang, Fabrication and thermal conductivity of copper matrix composites reinforced by tungsten-coated carbon nanotubes, Int. J. Min. Met. Mater. 19 (5) (2012) 446-452. https://doi.org/10.1007/s12613-012-0577-3

[23] R.R. Jiang, X.F. Zhou, Z.P. Liu, Electroless Ni-plated graphene for tensile strength enhancement of copper, Mat. Sci. Eng. A 679 (2017) 323-328. https://doi.org/10.1016/j.msea.2016.10.029

[24] Q.H. Hu, X.T. Wang, H. Chen, Z.F. Wang. Synthesis of Ni/graphene sheets by an electroless Ni-coating method, New Carbon Mater. 27 (1) (2012) 35-41. https://doi.org/10.1016/S1872-5805(12)60003-1

[25] Y.R. Wang, Y.M. Gao, J. Takahashi, Y. Wan, M.T. Li, B. Xiao, Y.Q. Zhang, et al., Investigation of modification of Cu-Ni-graphite composite by silver, Mater. Chem. Phys. 239 (2020) 121990. https://doi.org/10.1016/j.matchemphys.2019.121990

[26] H. Xu, J.H. Chen, S.B. Ren, X.B. He, X.H. Qu, Sintering behavior and thermal conductivity of nickel-coated graphite flake/copper composites fabricated by spark plasma sintering, Int. J. Min. Met. Mater. 25 (4) (2018) 459-471. https://doi.org/10.1007/s12613-018-1592-9

[27] H.D. Li, Y.L. Xia, M. Xie, C. Shi, J.B. Lei, Graphene nanoplatelets reinforced NiCu composite manufactured by laser melting deposition, J. Alloy Compd. 929 (2022) 167261. https://doi.org/10.1016/j.jallcom.2022.167261

[28] D.D. Zhang, Z.J. Zhan, Preparation of graphene nanoplatelets-copper composites by a modified semi-powders method and their mechanical properties, J. Alloy Compd. 658 (2015) 663-671. https://doi.org/10.1016/j.jallcom.2015.10.252

[29] D.B. Xiong, M. Cao, Q. Guo, Z.Q. Tan, G.L. Fan, Z.Q. Li, Graphene-and-copper artificial nacre fabricated by a preform impregnation process: bioinspired strategy for strengthening-toughening of metal matrix composite, Acs Nano. 9 (7) (2015) 6934-6943.

https://doi.org/10.1021/acsnano.5b01067

[30] L.L. Meng, X.L. Wang, J.L. Ning, X.S. Hu, G.H. Fan, K. Wu, Beyond the dimensional limitation in bio-inspired composite: Insertion of carbon nanotubes induced laminated Cu composite and the simultaneously enhanced strength and toughness, Carbon. 130 (2018) 222-232. https://doi.org/10.1016/j.carbon.2018. 01.006

[31] W.Y. Tan, X.S. Jiang, Z.Y. Shao, H.L. Sun, Y.J. Fang, R. Shu, Fabrication and mechanical properties of nano-carbon reinforced laminated Cu matrix composites, Powders Technol. 395 (2021) 377-390. https://doi.org/10.1016/j.powtec.2021.09.072

[32] C.J. Huang, J.S. Peng, Y.R. Cheng, Q. Zhao, Y. Du, S.X. Dou, Ultratough nacre-inspired epoxy-graphene composites with shape memory properties, J. Mater. Chem. A 7 (6) (2019) 2787-2794. https://doi.org/10.1039/c8ta10725d

[33] P.M. Hunger, A.E. Donius, U.G.K. Wegst, Platelets self-assemble into porous nacre during freeze casting, J. Mech. Behav. Biomed. 19 (2012) 87-93. https://doi.org /10.1016/j.jmbbm.2012.10.013

[34] F. Luo, X.S. Jiang, H.L. Sun, D.F. Mo, Y.L. Zhang, R. Shu, High thermal and electrical properties of electroless graphene films reinforced Cu matrix laminated composites, J. Alloy Compd. 925 (2022) 166710. https://doi.org/10.1016/j.jallcom.2022.166710

[35] L. Jiang, G.L. Fan, Z.Q. Li, X.Z. Kai, D. Zhang, Z.X. Chen, An approach to the uniform dispersion of a high volume fraction of carbon nanotubes in aluminum powders, Carbon. 49 (6) (2011) 1965-1971. https://doi.org/10.1016/j.carbon.2011.01.021

[36] Y.S. Su, Z. Li, Y. Yu, L. Zhao, Z.Q. Li, Q. Guo, Composite structural modeling and tensile mechanical behavior of graphene reinforced metal matrix composites, Sci. China Mater. 61 (1) (2018) 112-124. https://doi.org/10.1007/s40843-017-9142-2

[37] Z. Li, Q. Guo, Z.Q. Li, G.L. Fan, D.B. Xiong, Y.S. Su, Enhanced mechanical properties of graphene (reduced graphene oxide)/aluminum composites with a bioinspired nanolaminated structure, Nano. Lett. 15 (12) (2015) 8077-8083. https://doi.org/10.1021/acs.nanolett.5b03492

[38] W.T. Huo, C.X. Lei, Y. Du, G. Chang, M. Zhu, B. Chen, Superior strength-ductility synergy of ($TiC+Ti_5Si_3$)/Ti composites with nacre-inspired architecture, Compos. Part B Eng. 240 (2022) 109991. https://doi.org/10.1016/j.compositesb.2022.109991

[39] Y.L. Xue, W.G. Chen, J.J. Wang, L.L. Dong, Q. Zhao, Y.Q. Fu, Formation mechanism and

cohesive energy analysis of metal-coated graphene nanocomposites using in-situ co-reduction method, Materials. 11 (11) (2018) 2071. https://doi.org/10.3390/ma11112071

[40] Q. Liu, X.B. He, S.B. Ren, C. Zhang, T.T. Liu, X.H. Qu, Thermophysical properties and microstructure of graphite flake/copper composites processed by electroless copper coating, J. Alloy Compd. 587 (2014) 255-259. https://doi.org/10.1016/j.jallcom. 2013.09.207

[41] J.H. Zhao, P. Li, Q. Tang, Y.Q. Zhang, J.S. He, K. He, Influence of metal-coated graphite powders on microstructure and properties of the bronze-matrix/graphite composites, J. Mater. Eng. Perform. 26 (2) (2017) 792-801. https://doi.org/10.1007/s11665-016-2495-4

[42] J.H. Chen, S.B. Ren, X.B. He, X.H. Qu, Properties and microstructure of nickel-coated graphite flakes/copper composites fabricated by spark plasma sintering, Carbon. 121 (2017) 25-34. https://doi.org/10.1016/j.carbon.2017.05.082

[43] Y. Huang, X.Y. Peng, Y.W. Yang, H.W. Wu, X. Sun, X.P. Han, Electroless Cu\Ni plating on graphite flake and the effects to the properties of graphite flake/Si/Al hybrid composites, Met. Mater. Int. 24 (5) (2018) 1172-1180. https://doi.org/ 10.1007/s12540-018-0052-4

[44] R. Andrews, D. Jacques, M. Minot, T. Rantell, Fabrication of carbon multiwall nanotube/polymer composites by shear mixing, Macromol. Mater. Eng. 287 (6) (2002) 395-403. https://doi.org/10.1002/1439-2054(20020601)287:6<395::AID-MAME395>3.0.CO;2-S

[45] H. Choi, A. Bor, S. Sakuragi, J. Lee, H.T. Lim, The grinding behavior of ground copper powders for Cu/CNT nanocomposite fabrication by using the dry grinding process with a high-speed planetary ball mill, J. Korean Phys. Soc. 68 (1) (2016) 147-153. https://doi.org/10.3938/jkps.68.147

[46] E.B. Modin, E.V. Pustovalov, A.N. Fedorets, A.V. Dubinets, B.N. Grudin, V.S. Plotnikov, Atomic structure and crystallization processes of amorphous (Co,Ni)- P metallic alloy, J. Alloy Compd. 641 (2015) 139-143. https://doi.org/10.1016/j.jallcom.2015.04.060

[47] G.Y. Li, W.M. Jiang, F. Guan, J.W. Zhu, Z. Zhang, Z.T. Fan, Microstructure, mechanical properties and corrosion resistance of A356 aluminum/AZ91D magnesium bimetal prepared by a compound casting combined with a novel Ni-Cu composite interlayer, J. Mater. Process. Tech. 288 (2020) 116874. https://doi.org/ 10.1016/j.jmatprotec.2020

[48] L. Fan, Q. Wang, P. Yang, H.H. Chen, H.P. Hong, W.T. Zhang, Preparation of nickel coating on ZTA particles by electroless coating, Ceram. Int. 44 (10) (2018) 11013-11021.

https://doi.org/10.1016/j.ceramint.2018.03.055

[49] K.C. Chen, W.W. Wu, C.N. Liao, L.J. Chen, K.N. Tu, Observation of atomic diffusion at twin-modified grain boundaries in copper, Science. 321 (5892) (2008) 1066-1069. https://doi.org/10.1126/science.1160777

[50] X. Gao, H.Y. Yue, E.J. Guo, H. Zhang, X.Y. Lin, L.H. Yao, Mechanical properties and thermal conductivity of graphene reinforced copper matrix composites, Powders Technol. 301 (2016) 601-607. https://doi.org/10.1016/j.powtec.2016.06.045

[51] M.X. Li, H.W. Che, X.Y. Liu, S.X. Liang, H.L. Xie, Highly enhanced mechanical properties in Cu matrix composites reinforced with graphene decorated metallic nanoparticles, J. Mater. Sci. 49 (10) (2014) 3725-3731. https://doi.org/10.1007/s10853-014-8082-x

[52] X. Zhang, S.F. Li, B. Pan, D. Pan, S.Y. Zhou, S.H. Yang, A novel strengthening effect of in-situ nano Al_2O_{3w} on CNTs reinforced aluminum matrix nanocomposites and the matched strengthening mechanisms, J. Alloy Compd. 764 (2018) 279-88(2018). https://doi.org/10.1016/j.jallcom.2018.06.006

[53] B. Chen, J. Shen, X. Ye, H. Imai, J. Umeda, M. Takahashi, Solid-state interfacial reaction and load transfer efficiency in carbon nanotubes (CNTs)- reinforced aluminum matrix composites, Carbon. 114 (2016) 198-208. https://doi.org/10.1016/j.carbon.2016.12.013

[54] Y.Y. Jiang, Z.Q. Tan, G.L. Fan, L. Wang, D.B. Xiong, Q. Guo, Y.S. Su, Z.Q. Li, D. Zhang, Reaction-free interface promoting strength-ductility balance in graphene nanosheet/Al composites, Carbon. 158 (2019) 449-455. https://doi.org/10.1016/j.carbon.2019.11.010

[55] Z.J. Hu, R.F. Guo, S.M. Chen, Q. Jin, P. Shen, Synthesis of damage-tolerant Cu-matrix composites with nacre-inspired laminate-reticular hierarchical architecture via tuning compositional wettability, Scripta Mater. 18 (2020) 312-316. https://doi.org/10.1016/j.scriptamat.2020.05.029